An Investigation of Flow Separation and Aerodynamic Controls at Hypersonic Speeds

L. G. KAUFMAN II,* L. MECKLER,† AND S. A. HARTOFILIS‡
Grumman Aircraft Engineering Corporation, Bethpage, N. Y.

Flow separation and its effects on control characteristics were investigated for Mach 5 to 21 flows over simple geometries and some typical hypersonic flight configurations with aerodynamic controls. Similar to supersonic flows, hypersonic flow separation ahead of flaps on a flat plate, and the resulting pressure and heating rate distributions depend strongly on flow conditions and model geometry (particularly finite span effects). Adverse pressure gradients can be propagated far upstream (particularly for the thick hypersonic boundary layers) and can cause separation far ahead of flaps and fins. "Breakaway" separation from sharp expansion corners was also found to depend on the eventual existence of adverse pressure gradients. Aerodynamic controls were effective for the flight configurations tested, but had highly nonlinear characteristics, partly because of extensive regions of flow separation. As for the simpler geometries, extremely high pressures and heating rates occur locally at reattachment on the control surfaces.

Introduction

SUDDEN and large changes in aerodynamic control characteristics frequently result when the airflow separates from a surface. The problem of flow separation, important for low-speed flows, is even more severe for hypersonic flows because of the high energy levels involved. Extensive regions of separated flow can severely affect aerodynamic heating rates and pressure distributions. The need for a clear understanding of these effects, for the future design of controllable hypersonic vehicles, led to the research investigation described herein.

Because of the complexity of the phenomena, there are no satisfactory analytic methods for predicting hypersonic flow separation. Further, empirical methods were hindered by the general lack of hypersonic data. The investigation undertaken was principally experimental in nature for two reasons: first, to help satisfy the immediate need for typical hypersonic flow control data; and second, to provide the broad base of experimental data required for the future development of analytical methods used to estimate separation effects and aerodynamic control characteristics in hypersonic flows.

A comprehensive literature survey,[1] made at the onset of the investigation, was helpful for planning the experimental program. Results from the extensive test program were presented in a series of Air Force data reports that contain plots of all the pressure, aerodynamic heating rate, force, moment, and flap load data. The over-all program is described in an Air Force report that also contains a synopsis of the information on hypersonic aerodynamic controls available in the literature.[2] Several important problem areas pertinent to the design of controllable hypersonic vehicles were revealed. This paper summarizes some results and presents salient aspects of the investigation.

Test Program

Simple geometries were used to provide a better understanding of the fundamental types of separated flows, thus permitting a better insight into the separation effects on the more complicated configurations. The investigation of the simple flow geometries included: separation ahead of ramp-shaped flaps on flat plates, leading-edge separation and flows over sharp expansion corners, and interactions due to flows past wedge-shaped fins mounted on flat plates. The typical flight configurations were a clipped-delta-wing body combination and a pyramidal shape with triangular cross section. As indicated in Table 1, each model had several geometric variations and was tested through a wide range of freestream Mach numbers M_∞ and Reynolds numbers Re_∞. The data were obtained from tests performed (October 1962 through April 1964) in the large AEDC von Karman wind tunnels (A, B, and Hotshot 2), and in the Grumman Hypersonic Shock Tunnel.

In addition to the wide ranges of stream conditions, the models were tested through wide angle of attack ranges ($-54° \leq \alpha \leq +54°$), and the various aerodynamic controls were tested at many different settings. Trailing-edge flaps on the flight configurations were deflected at various angles from $-40°$ to $+40°$, and flaps on the flat plate models were deflected at angles up to 90°. To make optimum use of the continuous wind-tunnel test time, the aerodynamic con-

Table 1 Outline of test program

Configuration	M_∞	$Re_\infty/10^6$ ft	Data[a]
Flat plate with full and partial-span flaps, with and without end plates and internal cooling	5	1.1 to 6.6	p, photo
	8	1.1 to 3.3	p, $\dot{q}$, photo
	13	~0.1	p, $\dot{q}$, photo
	19	~0.1	p, $\dot{q}$, photo
Flat plates forming convex corners, various expansion angles and corner radii	5	1.1 to 6.6	p, photo
	8	1.1 to 3.3	p, $\dot{q}$, photo
	13	0.1 to 0.2	p, $\dot{q}$, photo
	19	~0.1	p, $\dot{q}$, photo
Flat plate with wedge-shaped fins, sharp and blunt leading-edge fins of two heights	5	1.1 to 6.6	p, photo
	8	1.1 to 3.3	p, $\dot{q}$
	13	~0.2	p, $\dot{q}$, photo
	19	~0.1	p, $\dot{q}$, photo
Delta-wing-body combination with flaps, with and without tip fins and spoiler	5	2.3 to 5.0	p, F, photo
	8	0.8 to 3.3	p, $\dot{q}$, F
	19	~0.1	p, photo
Pyramidal lifting body with trailing-edge flaps, with and without canards and ventral fin	5	0.7 to 6.6	p, F, f, photo
	8	1.1 to 3.3	p, $\dot{q}$, F, f, photo
	21	~0.1	p, $\dot{q}$, photo

[a] $p \sim$ pressure; $\dot{q} \sim$ heat transfer; $F \sim$ 6-component force and moment; $f \sim$ flap hinge and twisting moments and normal load; photo ~ flow photographs or high-speed motion pictures.

† Presented as AIAA Preprint 65-753 at the AIAA/RAeS/JSASS Aircraft Design and Technology Meeting, November 15–18, 1965, Los Angeles, Calif.; submitted December 3, 1965; revision received June 29, 1966. Supported primarily by the Air Force Flight Dynamics Laboratory under Contract AF 33(616)-8130.

* Research Scientist. Member AIAA.
† Research Engineer. Member AIAA.
‡ Research Engineer; now with Blair and Co., Mineola, N. Y. Member AIAA.

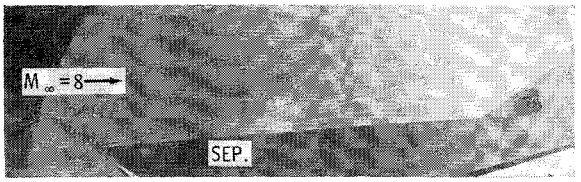

a) Re_∞/ft 1.1 million

b) Re_∞/ft. 3.3 million

Fig. 1 Shadowgraph photographs for Mach 8 flows over full-span 30° trailing-edge flaps on a flat plate at 5° angle of attack.

trol surfaces on several of the models were remotely actuated. Table 1 indicates the types of data obtained for the various flow models in each wind tunnel.

At Mach 8, heating rates were obtained from transient temperatures measured during the initial heating of cold-wall models. The use of honeycomb sandwich construction for the planar portions of these models avoided many of the usual problems associated with thin wall heat-transfer measurements without compromising the accuracy of the heat-transfer data. Several flow visualization techniques were used that provided schlieren, shadowgraph, and oil film flow photographs. In one instance, high-speed motion pictures were used to record the charring of a thin coat of ordinary white enamel paint sprayed on the Hotshot 2 model, which indicated regions of high aerodynamic heating rates.

Flows over Flaps

In hypersonic flows, effective aerodynamic controls usually involve compressions of the local stream flow, and thus give rise to shock-induced separation. Pressure rises, because of trailing-edge flaps for example, propagate through the boundary layer and can cause separation far upstream of the flap. The extent of the separated flow region depends on the nature of the boundary layer, stream conditions, wall temperature, and model geometry. Further, the flap can experience extremely high local heating rates and pressures if the flow reattaches to the control surface.

Pressure and aerodynamic heating rate distributions were obtained at several spanwise stations for flows over full- and partial-span trailing-edge flaps mounted on flat plates, both with and without end plates. One model was internally cooled so that wall temperature effects on the pressure distributions could be investigated. This was particularly desirable at Mach 8, because heating rates were obtained while the model was cool, whereas corresponding pressures were measured on comparatively hot-wall models.

The strong dependence of separation on the nature of the boundary layer is indicated by the sample shadowgraphs of Fig. 1. For the test conditions given in the figure, laminar separation near the plate leading edge was observed for a unit freestream Reynolds number of 1.1×10^6, whereas transitional separation was observed for $Re_\infty/\text{ft} = 3.3. \times 10^6$. High-speed schlieren motion pictures, when reviewed at reduced speed, showed that the separated flows were stable. Sample centerline distributions of aerodynamic heating rates $\dot{q}$-(Btu/ft^2 sec) vs nondimensional streamwise surface distance X are presented in Fig. 2. The heat-transfer rates decrease from their leading-edge values, drop sharply to almost zero at the separation point, increase gradually within the separated flow zone, and increase abruptly at reattachment on the flap surface. As shown in Fig. 2, the heat-transfer rates and the extent of separation are strongly dependent on the Reynolds number. For increasing Reynolds numbers, the separation point moves downstream and reattachment moves upstream. The heat-transfer distributions increase proportionately with Reynolds numbers and are maximum at reattachment. The curves shown in Fig. 2 are drawn through fairly dense ($\Delta X = 0.03$) data points, and indicate the maximum heat-transfer rates measured; however, because of the large gradients, the true peak values may be somewhat larger.

Although streamwise distributions of pressures and heating rates did not vary appreciably for different spanwise locations,[2] end plates altered the measured distributions significantly (Figs. 2 and 3). The end plates prevent venting of the highly vortical, separated, reverse flow and delay reattachment. Thus they substantially increase the amount of trapped flow in the separated region and lead to a larger dividing streamline angle at separation. This results in larger pressures on the flat plate surface and generally lower pressures on the flap surface (see Fig. 3).

Finite span effects were also examined using a partial-span trailing-edge flap. As expected, the separated flow region is smallest for the partial-span flap and largest when the full-span flap is end plated (Fig. 3). Lateral venting of the vortical reverse flow in the separated region ahead of the flap is easiest for the partial-span flap, but is essentially prevented by the end plates.

Transverse flow effects are more pronounced for lower Reynolds numbers, higher Mach numbers, and higher pressure rises (larger flap deflections δ). For Mach 8 flows over 45° flaps with end plates, the flow separates near the leading edge of the flat plate and does not reattach until near the flap trailing edge.[2] The extent of separation and end-plate effects are small for 20° flaps, and are negligible for 10° flaps. For Mach 16 flows, Miller, Hijman, and Childs[4] observed similarly large end plate effects for 30° flaps, less pronounced effects for 22.5° flaps, and negligible end plate effects for 15° flaps.

Also indicated in Fig. 3 are wall temperature effects on the pressure distribution. In general, cooling the wall delayed

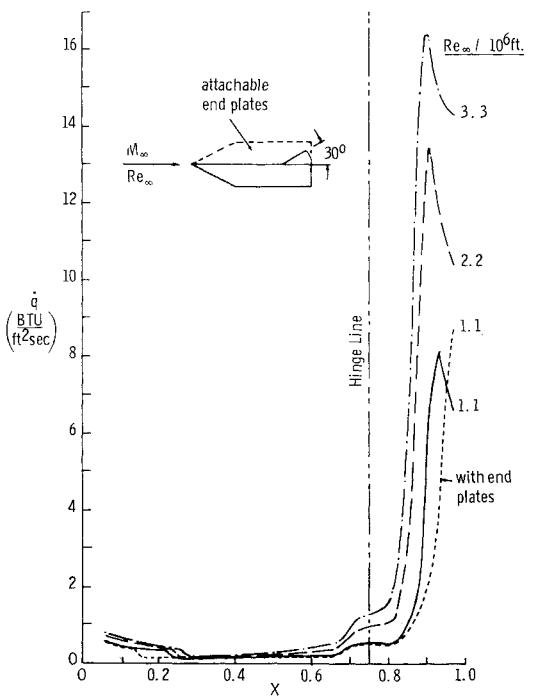

Fig. 2 Centerline distributions of aerodynamic heating rates for Mach 8 flows over flat plates with full-span trailing-edge flaps.

separation and reduced its extent, except when the cooling was sufficient to change the character of the boundary layer. Thus, as for the sample shown in Fig. 3, cooling delayed separation somewhat, but the laminar reattachment for the cooled wall was downstream of the corresponding reattachment point for the noncooled wall.[2]

Without end plates, the maximum flap pressures exceeded the inviscid wedge values in several instances (Figs. 3 and 4). Mach number effects are quite pronounced for the location of separation and the pressure coefficients on the flap surface, especially near reattachment. Very high pressures were measured near reattachment on the flap when the flat plate surface was windward. The high local loads at reattachment are caused by the comparatively gradual compression of the flow through a series of oblique shock waves, thereby avoiding the strong shock wave losses of a one-step compression. A combination of just two shock waves, one at separation and one at reattachment, results in a larger static pressure downstream of reattachment on the flap surface than would result if there were no separation and just one stronger shock wave at the flap hinge line that gave the same total turning angle.

In general, the separation effects described herein become more pronounced for the thicker boundary layers (because of either lower Re_∞ or higher M_∞ values) and higher pressure rises (larger flap deflections). For the same Reynolds number, the extent of separation increases with Mach number (Fig. 4); and at the higher Mach numbers we observed an increased importance of Reynolds number effects. Thus, when the unit freestream Reynolds numbers were decreased from 3.3 to 1.1 million, the extent of separation increased more for the Mach 8 flows than for the Mach 5 flows. Although Miller, Hijman, and Childs[4] observed an apparent reverse trend of Reynolds number effects for Mach 16 (increasing extent of separation with increasing Reynolds number), our results indicated no such reversal. We believe that the apparent reverse trend of Reynolds number effects at Mach 16 results from the predominance of favorable pressure gradients caused by viscous leading-edge effects.

Flows over Expansion Corners

It had been conjectured, primarily intuitively, that high-speed flows could not negotiate sharp expansion corners without breaking away from the surface and forming at least a small bubble of separated flow immediately downstream

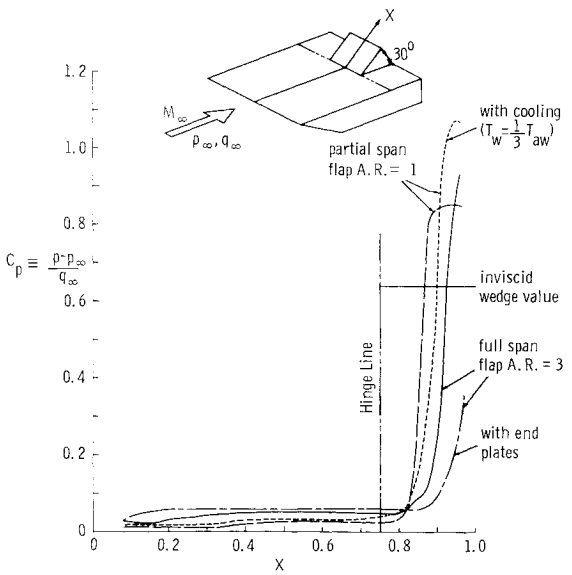

Fig. 3 Centerline pressure coefficient distributions for Mach 8 flows over flat plates with 30° trailing-edge flaps, Re_∞/ft = 1.1 million.

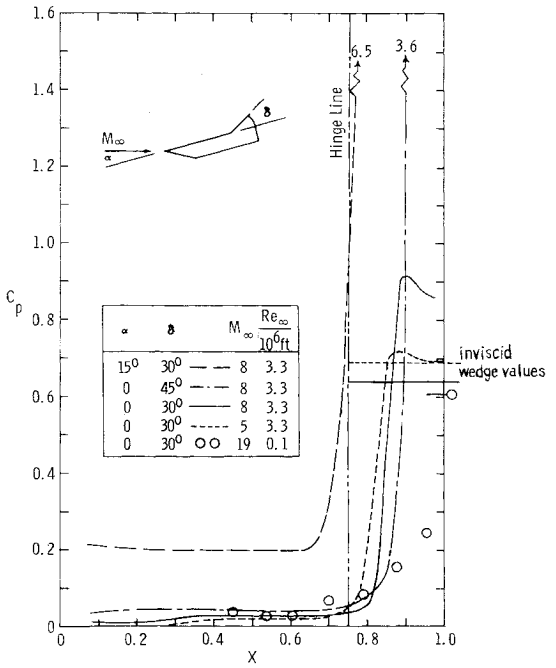

Fig. 4 Centerline pressure coefficient distributions for flat plates with full-span flaps.

of the corner. However, for supersonic flows over expansion corners, the streamwise pressure gradient is negative, and therefore favorable for attached boundary layers. Because the local pressure gradient is favorable in the inviscid sense, there was controversy as to the cause of breakaway separation.[1]

Positive pressure gradients are required for separation according to standard boundary-layer methods, but the basic assumption of these methods is that the surface curvature be small compared to the boundary-layer thickness, and this is violated at the sharp corner. Further, when nondimensionalizing the curvilinear Navier-Stokes equations[5] and performing an order-of-magnitude analysis, the pressure variation across the boundary layer is found to be of the same order of magnitude as the pressure itself [$\Delta p = 0(p)$] for small corner radii [$r = 0(\delta)$]. Thus, in contrast to the standard boundary-layer result, there are large pressure gradients normal to the surface, and the normal momentum equation must be retained for flows over sharp expansion corners. After abandoning standard boundary-layer methods, many approaches to the problem have been based on simplified assumptions that avoid the sharp corner singularity.[2] Some of the more promising approaches correctly predict the boundary-layer characteristics downstream of the corner, but all mask the nature of the flow in the immediate vicinity of the corner.

Experimentally, we investigated flow separation from the leeward side of the sharp leading edge using the flat plate models mentioned in the preceding section. The flow was observed (through a ground-glass shadowgraph viewing screen) as the flat plate surface was slowly pitched to leeward and then returned to zero angle of attack. As the plate surface became more leeward, the separation point moved, comparatively rapidly, upstream to the sharp leading edge of the flat plate, as sketched in Fig. 5a. Although rapid, the upstream movement of the separation point was continuous; and moreover, the process was reversible as the angle of attack was returned to zero. The procedure was repeated for different freestream Reynolds numbers (at Mach 8), and pressure distributions were recorded at discrete angles of attack. There was no sudden breakaway of the flow from the leading edge, but rather, a rapid extension of the separation flow region attributed to the eventual dowstream pressure

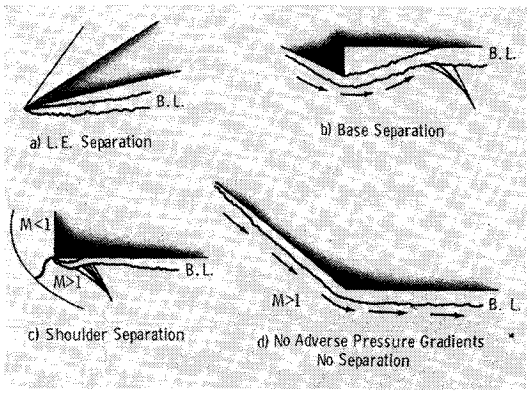

Fig. 5 Sketches of flows over expansion corners.

rise required to recompress the flow at the trailing edge of the model.

Separation behind rear-facing steps and ramps, as sketched in Fig. 5b, also can be attributed to the upstream propagation of adverse pressure gradients through the subsonic portion of the boundary layer. To assess the importance of adverse pressure gradient effects on breakaway separation, flows over simple 30° and 40° expansion corners, for which there were no downstream recompressions, were investigated.[2] The models had interchangeable round and sharp corners, and large aspect ratios to provide essentially two-dimensional flow along their center planes. Surface pressures were measured upstream and downstream of the expansion corners for various freestream Mach numbers and angles of attack (referenced to the flat plate surface downstream of the corner). When this surface was windward, or parallel to the freestream flow as sketched in Fig. 5d, there were no downstream pressure rises, and there was no evidence of any flow separation for all cases where the wedge leading-edge shock was attached.

In some cases, when the wedge leading-edge shock is detached for positive angles of attack, there is a characteristic dip in the pressure distribution immediately downstream of the corner, followed by a recompression. For subsonic wedge flows there is a sonic line at the corner on the upstream surface. Expansion waves from the corner are reflected from the sonic line as compressions and are responsible for the recompressions.[2] For very strong recompressions, like those on a flat-nosed plate (90° expansion corner at shoulder), the adverse pressure gradient due to the recompression can be strong enough to cause a small separated flow bubble immediately downstream of the corner,[6] as sketched in Fig. 5c. This again shows the dependence of separation on adverse pressure gradients.

Rear- and forward-facing Stanton tubes located immediately downstream of the 30° and 40° expansion corners gave no evidence of any separation. For all test conditions, all forward-facing tubes measured higher total pressures than the corresponding rear-facing tubes. Further, the rear-facing tubes gave pressures lower than the local surface static pressures. These results are the prime experimental evidence that there was no separation downstream of the sharp expansion corners. In addition, distributions of heating rates and flow pictures showed no separation downstream of the sharp expansion corners. We conclude that separation does not occur without adverse pressure gradients, although the pressure rises can be located far downstream of the separation points.

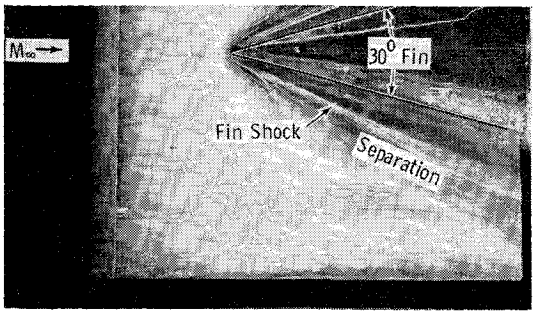

Fig. 6 Oil film flow photograph of fin plate interaction for $M_\infty = 5$ and $Re_\infty/\text{ft} = 6.6$ million.

Fin Plate Interactions

The dominant mechanism in fin plate interactions is the separation of the plate boundary layer by the fin shock wave. There are three basic modes in which this separation can take place, and many combinations of them may be present in any given interaction.

The first mode occurs near the fin leading edge, where the thickness of the inviscid shock layer on the fin is very small relative to the length of the separated boundary layer on the plate. The pressure rise due to the fin shock is propagated upstream through the boundary layer, and separation occurs far ahead of the fin. This mode has been observed on plates upstream of both blunt and sharp fins, although the details are different in the two cases. Three-dimensional effects are always of first-order importance in this mode, and there are no satisfactory methods for predicting the flow characteristics, except by purely empirical means.

The oil film flow photograph of Fig. 6 presents evidence of two modes of interaction separation caused by a small fin mounted on a flat plate. The region of separated flow near the forward portion of the fin is characteristic of the first mode of interaction separation; it is predominantly three dimensional. Near the model trailing edge, the interaction is of the second mode, and for this type of interaction the flow is nearly conical in nature. In this mode, the fin shock-layer thickness is comparable to the separation zone length measured normal to the local fin surface. The presence of the fin is an essential part of the structure of the separation zone in this mode, and the separation line on the plate is not, in general, parallel to either the fin or the fin shock.

The third basic mode occurs when the shock wave is sufficiently far from the fin so that the separated boundary layer on the plate can reattach without significant influences from the presence of the fin. In this mode the fin acts simply as a shock generator, and the problem reduces to the pseudo-two-dimensional problem of a swept planar shock separating a boundary layer.[7] The fin plate junction, far enough downstream of the leading edge, poses a streamwise corner boundary-layer problem for the reattached flow downstream of the fin shock. However, at hypersonic speeds the fin shock is close to the fin surface, and generally the interaction cannot be split into separate incident shock and corner flow boundary-layer problems. Thus, the subject investigation was concerned primarily with the first two modes of fin plate interaction separation.

Spanwise pressure and heating rate distributions were obtained on the fin and plate surfaces for wedge-shaped fins having different heights and sharp or cylindrically blunted leading edges. Typical Mach and Reynolds numbers effects on the interaction pressures and heating rates are indicated in Fig. 7 for flows past a small fin (30° wedge with sharp leading edge) mounted on a flat plate. The pressure rise due to the fin shock is propagated far outboard and causes substantial overpressures over a large portion of the plate surface, particularly for the thicker boundary layers (smaller Reynolds number values).

The data presented in Fig. 7 are representative of those obtained for the second mode of interaction separation. In many cases, particularly for fins with blunt leading edges, the interaction was predominantly three dimensional in character (first mode). Although not amendable to theoretical

analyses at present, pressures and heating rates were measured for a wide variety of flow conditions and can readily be used for engineering estimates. Particularly noteworthy in this aspect are the high pressures and heating rates observed on the cylindrically blunted fin leading edges in the immediate vicinity of reattachment. In some cases the peak values were more than three times larger than the stagnation values of the pressures and heating rates measured on the cylindrical leading edge outside of the interaction region.[2]

Hypersonic Aerodynamic Controls

Controls are required to provide maneuvering capability and trim for any flight vehicle. The most common type of control used in the atmosphere is an aerodynamic surface, but the application of these surfaces to hypersonic flight vehicles presents many formidable problems. At very high altitudes, thick boundary layers, low dynamic pressures, and extensive separated flow regions induced by deflected controls can greatly reduce the effectiveness of aerodynamic controls. The over-all problem is aggravated by the large ranges of speed and angle of attack encountered by hypersonic flight vehicles.

Although many control configurations are possible, the general problem areas can be investigated using a few different types of controls on simplified configurations. With this in mind, a delta-wing-body combination and a pyramidal lifting body with a shallow triangular cross section and a highly swept delta-wing planform were chosen as representative hypersonic flight configurations. The essential features affecting control characteristics were similar for the two basic configurations; they are described herein using selected data for the delta-wing body combination.

As shown in Fig. 8, the delta wing has a spherically blunted apex, cylindrically blunted leading edges, a blunt base, and clipped tips. The overslung body had a half conical foresection and a half-cylindrical aftersection joined at the shoulder by a spherical fairing. The control surfaces, a deflectable apex and independently operated partial-span trailing-edge flaps, had maximum travel angles of $\pm 20°$ and $\pm 40°$, respectively. The configuration also had attachable clipped delta tip fins, a full-span plug-type trailing-edge spoiler, and a wedge section designed to fit between the partial-span flaps to form a full-span flap on the lower surface of the wing. The term "flap" is used to denote controls with a general type of geometry, rather than their function. Thus trailing-edge elevators, ailerons, or elevons are all referred to as flaps.

The sign convention for denoting the angle of attack and the control deflection angle can be obtained from the basic model, a delta wing with an overslung body. The angle of attack α is referenced to the lower flat plate surface of the wing, and is positive when the flat plate surface is windward. Positive trailing-edge flap deflections δ are obtained by deflecting the trailing edge down. The sign convention for the forces and moments is shown in Fig. 8. The basic wing-body combination provides control information for configurations having either overslung or underslung bodies. The positive angle of attack data for the overslung body provides data for the underslung body at negative angles of attack, with appropriate reversal in the sign of the flap deflection angles.

Sample Mach 8 data for the static longitudinal aerodynamic characteristics for symmetric deflections of the trailing-edge flaps are shown in Fig. 9. The flaps are effective in producing force increments through the entire angle of attack range, and are most effective when deflected into the incident flow. The normal force increments increased with angle of attack for positive flap deflections at positive angles of attack and negative flap deflections at negative angles of attack up to angles of attack of about $+30°$ and $-30°$, respectively. Beyond these angles of attack the incremental normal force coefficients decreased with increasing angle of attack. At high angles of attack and large flap deflection angles, the flap is almost normal to the flow, and contributes little to the normal force coefficients. From Fig. 9, for the 20° flap deflection case, the peak normal force increment occurs at $\alpha \approx 40°$, while for the 40° flap deflection case, the peak normal force increment occurs at $\alpha \approx 25°$. The flaps produce incremental normal force coefficients even when they are deflected out of the flow; in part this is because of the pressure relief on the windward side of the model.

With the moment reference center at 60% of the virtual root chord, the basic configuration was statically stable at Mach 8 for the middle portions of the angle of attack range for all flap deflections tested. Although trim points were found for all flap deflection angles at Mach 8, there are large ranges of angle of attack where the stability of the configuration, using these flaps, varies from marginal to neutral.

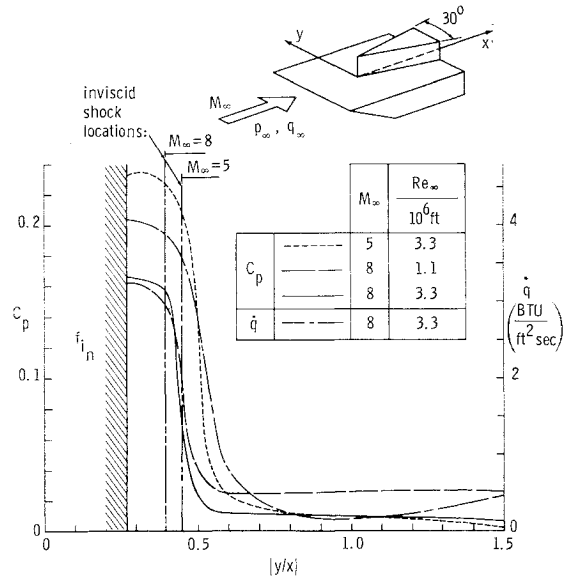

Fig. 7 Pressure coefficients and heating rates on flat plate due to boundary-layer interaction with shock wave generated by a small wedge-shaped fin.

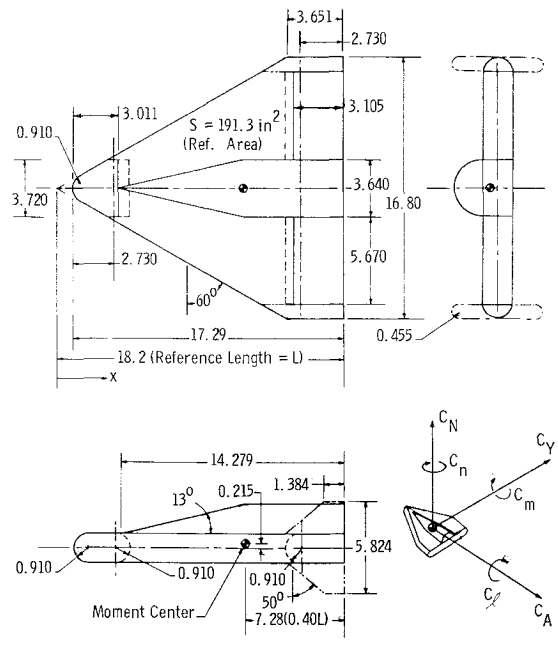

Fig. 8 Force and moment model of winged re-entry configuration and sign convention for force and moment coefficients.

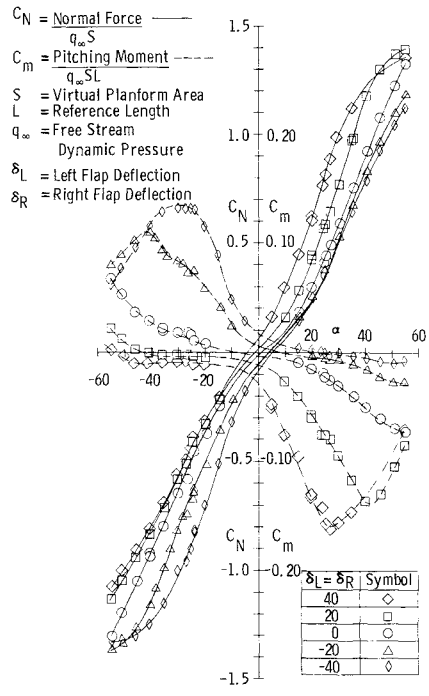

Fig. 9 Normal force and pitching-moment coefficients for delta-wing-body combination with symmetric flap deflections for M_∞ = 8 and Re_∞/ft = 2.3 million.

Strong pitch-up (indicated by a decrease in restoring moment) is observed when the flaps are deflected into the flow. The angle of attack at which pitch-up occurs is strongly dependent on the flap deflection angles. This dependence is caused by the extensive separated flow areas induced by large flap deflection angles. Flow separation tends to limit the pressure rise on the flap, but induces a strong pressure rise on the wing forward of the flap hinge line. The resulting forward movement of the center of pressure sharply decreases the pitching moments. This pitch-up tendency is also noted at the negative flap deflection angles, but at higher angles of attack.

In the angle of attack range where the flaps are deflected into the flow, and prior to the onset of pitch-up, these flaps are effective generators of restoring moments for both the overslung and underslung configurations. Because of the marginal stability when the flaps are deflected out of the flow, the trim points are not well defined.

The addition of tip fins to this configuration increased the slope of the normal force coefficient curve and increased the effectiveness of the flaps. The slope of the resulting pitching moment curve became more negative and the extent of the marginal stability range was decreased. The presence of the fins narrowed the latitude of trim angles associated with flap deflection. These comparisons indicate strong beneficial effects caused by wing-fin interference and end plating.

Comparisons were obtained between the partial-span trailing-edge flaps and a full-span flap for a deflection angle of +20°. A full-span spoiler, having the same height as the +20° flap, and a deflectable apex also were investigated. The added control surface area of the full-span flap produced positive normal force increments and stronger restoring moments. The full-span spoiler was effective in producing increments of normal force and restoring pitching moment when it was exposed to the flow. The effectiveness, approximately the same as the full-span flap, increased with increasing angle of attack in the angle of attack range of 0° to +25°. The deflectable apex, although it produced slight increments in normal force and pitching moments, was not as effective as the other controls investigated.

The lateral and directional characteristics of the aileron-type flaps on the basic configuration are shown in Fig. 10. The aileron controls are effective over the range tested whether they are deflected separately or differentially. Near $\alpha = 0$, the individually deflected flaps produce lower rolling moments and higher, adverse, yawing moments than the differentially deflected flaps. As the angle of attack is increased, and one of the differentially deflected flaps is shielded by the wing, the differences in response of both types of roll control diminish. The effectiveness increased with increasing control deflection and increasing angle of attack. The adverse yawing moment also increased with increasing control deflection and angle of attack, with the exception of the range around $\alpha = 0$ where differential flap deflections tended to minimize the adverse yawing moments. When both flaps are exposed to the flow they produce opposite (cancelling) yawing moments, except for the interference loads induced on the body that are generally quite small. The addition of the fins had little effect on the yawing moments (for zero sideslip angle) but did, in general, increase the rolling effectiveness; this was because of the beneficial effects of wing-fin interference.

We have also included a group of pressure and heat-transfer distributions (measured on the lower surface at the flap mid span) in order to provide a better understanding of the effects of control deflection and angle of attack on the aerodynamic characteristics (Fig. 11). These representative distributions do not necessarily indicate the peak values that were obtained. It is evident that control deflections produce large increases in pressure and heat transfer on the control itself. Moderate deflection angles and angles of attack ($0 \leq \alpha \leq 20°, 0 \leq \delta \leq 20°$) do not induce extensive separation. Large flap deflections induce separation far forward of the hinge line at all angles of attack, and at high angles of attack all flap deflections tested induced strong separation effects forward of the hinge line. The separated flow regions are highly three dimensional. These observations from the pressure distributions explain the loss in control effectiveness in the higher angle of attack and control deflection ranges because of the pressure decrease on the flap and the pressure increase on the wing forward of moment center caused by flow separation.

The heat-transfer data presented in Fig. 11 show extreme heating rate values on the flaps at high total flow deflection angles (angle of attack + flap deflection angle). In some cases the measured values exceeded those calculated at the blunt-nose stagnation point. This heating problem is a major stumbling block to the design and fabrication of effective hypersonic aerodynamic controls.

Conclusions

For hypersonic flows, Reynolds number, Mach number, pressure rise (flap deflection angle), model geometry, and wall

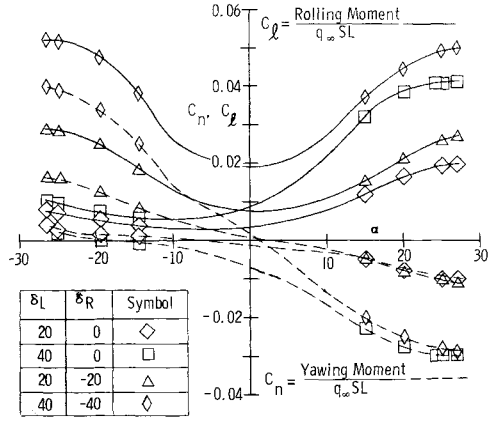

Fig. 10 Yawing and rolling moment coefficients for delta-wing-body combination with asymmetric flap deflections for M_∞ = 8 and Re_∞/ft = 2.3 million.

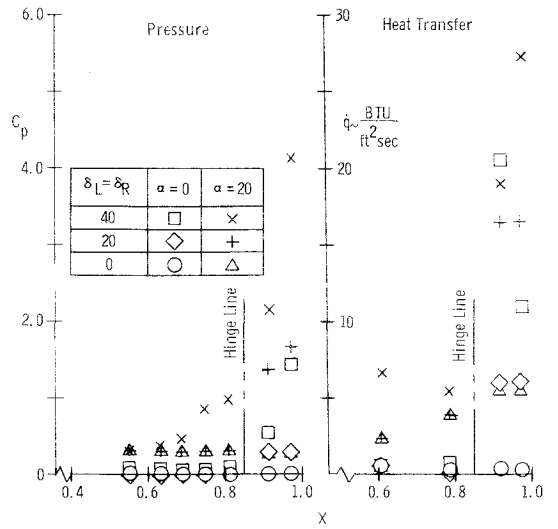

Fig. 11 Pressure coefficients and aerodynamic heating rate distributions on lower surface of delta-wing-body configuration at flap semispan station for $M_\infty = 8$ and $Re_\infty/\text{ft} = 3.3$ million.

temperature were found to affect strongly the extent and location of separation, which in turn strongly affects the aerodynamic heating rates and pressure distributions. Even for high-aspect-ratio flat plates with full-span trailing-edge flaps, the separated flow is essentially three dimensional in nature and strongly affected by finite span effects. End plating the model prevented venting of the reverse flow in the separation region and doubled the extent of separation. This greatly changed the chordwise pressure and heating rate distributions, increasing their values on the plate surface while decreasing their values on the flap surface.

Streamwise pressure and heating rate gradients are extremely large just upstream of reattachment and lead to exceptionally high pressures and heating rates downstream of reattachment on trailing-edge flaps. The pressures downstream of reattachment are considerably larger than the inviscid values calculated neglecting separation. As expected, these effects become more pronounced for the higher Mach number flows.

No breakaway flow separation was found in the complete absence of adverse pressure gradients. The eventual existence of an adverse pressure gradient, although far downstream of the separation point, is a necessary condition for separation.

The effect of interaction of a fin generated shock wave with the boundary layer on a flat plate is much greater for hypersonic flows than for supersonic flows. In supersonic flows, the region of separation on the plate surface is limited to the vicinity of the shock wave. In hypersonic flows, the separated flow region on the plate extends from the fin root to far outboard of the inviscid shock location. Particularly for the thick hypersonic boundary layers, the pressure rise due to the fin shock is propagated far outboard and causes substantial overpressures over a large portion of the plate surface.

The basic types of separation phenomena investigated for the flat plate models were evident in the pressure, heat-transfer, and force data obtained on the typical flight configurations. Aerodynamic surfaces of reasonable proportions were effective as control devices, but their characteristics were highly nonlinear, partly because of extensive regions of separation when the control surfaces were deflected into the flow. In these regions there are strong spanwise as well as streamwise gradients in the pressure and heating rate distributions. In many cases the peak pressures and heating rates recorded on trailing-edge flaps were more than twice as large as blunt-nose stagnation-point values. Large shifts in center of pressure locations, both spanwise and streamwise, can result from comparatively small changes in the model angle of attack or flap deflection. The flows are highly three dimensional and offer little hope for other than empirical solutions in the near future.

References

[1] Kaufman, L. G., II, Oman, R. A., Hartofilis, S. A., Meckler, L. H., Evans, W. J., and Weiss, D., "A review of hypersonic flow separation and control characteristics," Aeronautical Systems Division, ASD-TDR-62-168 (March 1962).

[2] Kaufman, L. G., II, Meckler, L. H., Hartofilis, S. A., and Weiss, D., "An investigation of hypersonic flow separation and control characteristics, Air Force Flight Dynamics Lab., AFFDL-TR 64-174 (January 1965).

[3] Meckler, L. H., "Instrumented honeycomb panels for aerodynamic heat transfer measurements," Grumman Research Department Memo. RM-282 (June 1965).

[4] Miller, D. S., Hijman, R., and Childs, M. E., "Mach 8 to 22 studies of flow separation due to deflected control surfaces," AIAA J. 2, 312–321 (1964).

[5] Schlichting, H., *Boundary Layer Theory* (McGraw Hill Book Company Inc., New York, 1955), p. 98.

[6] Sears, W. R. (ed.), *General Theory of High Speed Aerodynamics* (Princeton University Press, Princeton, N. J., 1954), Vol. VI, pp. 417 and 705.

[7] Martellucci, A. and Libby, P. A., "Supersonic flow about general three dimensional blunt bodies," *Heat Transfer Due to the Interaction Between a Swept Planar Shock Wave and a Laminar Boundary Layer*, Vol. II, Aeronautical Systems Division, ASD-TR-61-727 (October 1962).